Dcon/ Natl.

398

Paper presented at the AIAA National Summer Meeting,
Los Angeles, Calif., June 17-20, 1963

A PROGRESS REPORT ON THE AMES HYPERVELOCITY FREE-FLIGHT FACILITIES AND SOME OF THE CURRENT RESEARCH PROBLEMS BEING STUDIED IN THEM

By Alvin Seiff [1963]
National Aeronautics and Space Administration
Ames Research Center
Moffett Field, Calif.

SUMMARY

A description is given of the facilities developed at the Ames Research Center for experimental study of gas dynamics problems at speeds currently as high as 44,000 feet per second, and at air densities in the range from 0.0002 to 0.16 times sea-level atmospheric density. This range of conditions is achieved by combining in countercurrent operation a shock-tube wind tunnel with a light-gas gun. The test model launched from the gun flies upstream through the high velocity flow generated by the shock-tube wind tunnel. The operational problems of this equipment, while considerable, have been surmounted to a usable degree, and those that remain are primarily problems common to high-performance shock-tube wind tunnels.

This equipment has permitted the study of air radiation from the shock layer for speeds up to and above the escape velocity from earth, for both equilibrium and nonequilibrium conditions in the shock layer. It also provides an opportunity for studying the characteristics of ablating models, and these studies have shown the presence of additional radiation in appreciable quantities, both in the shock layer and the wake, attributable to the ablation products. The equipment was designed for measuring aerodynamic forces and moments as well, and, while these studies have not been emphasized thus far, stability and drag have been measured at speeds above 30,000 ft/sec and Mach numbers as high as 35. A

measurement of stagnation-point convective heating for a speed of 36,000 ft/sec has also been accomplished, by use of the flight time to onset of ablation as a measure of the heating rate.

INTRODUCTION

In the past 15 years, there has developed a considerable emphasis on free-flight testing of scale models for experimental studies of gas dynamics problems. The models are set in motion from light-gas guns up to very high velocities. This kind of experiment has permitted measurements at some conditions of speed and density not readily attainable by other techniques, and has also been used to study some gasdynamic properties and effects which are better studied in free flight than on fixed mounts. During this period, there has been a rapid increase in the speed of testing. The usefulness of the technique has stimulated the development of improved guns, and the development of improved guns has increased the usefulness of the technique. Today, with guns alone, we can test at speeds as high as 30,000 ft/sec (ref. 1), thus exceeding satellite speed in free flight laboratory experiments.

Another useful idea has been the combining of the free-flight model with a countercurrent supersonic air stream. This combination has been employed in the Ames supersonic free-flight wind tunnel (ref. 2) for a period of 15 years and has been the basis of both basic research and development testing at Mach numbers as high as 18, although at a total velocity of roughly 0.6 the value for free flight at this same Mach number in the atmosphere.

With the coming of the space age, there was a well recognized need for ground facilities to perform experiments up to and above 40,000 ft/sec. Because of the importance of gaseous radiation, ionization, dissociation, and other behavior of air around flight vehicles at these speeds, it was considered

important to test at the speed of interest rather than to attempt simulation of these effects at some lower speed. The free-flight model test with the light-gas gun fits in with this requirement, of course, but unfortunately falls somewhat short of the highest speed of interest, even now. It was logical to consider the application of the countercurrent air-stream technique to overcome this deficiency. The decision to apply this technique on a pilot scale was made at Ames Research Center in the spring of 1958.

The air streams employed in the earlier supersonic free-flight wind tunnel were cold reservoir streams and, as such, were limited to a maximum speed (on expansion to infinite Mach number) of about 2,500 ft/sec. For the much higher airspeeds desired here, a shock-tube wind tunnel was selected. With this type of equipment, tests at speeds up to 44,000 ft/sec have been made. Although the equipment developed for this purpose is still far from perfected, it has been used for a number of kinds of gasdynamic and heating experiments, and has developed far enough to warrant a progress report. The present purpose is to make such a report, to describe the existing systems, to review some of the operating problems, and to discuss some of the research applications.

The author would like to acknowledge the contributions of the many members of the Hypersonic Free-Flight Branch at Ames Research Center who collaborated in the work reported here.

SYMBOLS

E_t total radiative power per unit volume of the gas, watts/cm^3

h stream enthalpy, Btu/lb

I total nonequilibrium radiative power per unit area of the shock wave, watts/cm^2

M free-stream Mach number

p pressure, lb/in.^{2} or atmospheres, as noted

$\dot{q}$ stagnation-point heating rate, Btu/sec ft^2

r nose radius of curvature, ft

t time, milliseconds

T_S surface temperature at stagnation point, $^\circ$F

V free-stream velocity, ft/sec

x axial coordinate of test equipment, ft

ρ air density, slugs/ft^3

Subscripts

o sea level atmospheric condition

s stagnation value

t total

w wall value

∞ undisturbed free-stream value

FACILITIES

Description

Two versions of this equipment have been built and operated, referred to as the pilot and prototype. The pilot unit (ref. 3) has a test section 7 inches in diameter by 3 feet long, is driven by a 4-inch-diameter shock tube employing cold helium driver gas, and is equipped with a model launching gun 0.28 inch in bore diameter. This equipment has been used for gaseous radiation studies at speeds up to 33,000 ft/sec, reported in references 3, 4, and 5.

The prototype facility has a test section 40 feet long, suitable for gas-dynamic force and stability measurements as well as radiation measurements, and is shown sketched in figure 1. The over-all length of this equipment is slightly

over 200 feet. The driver and the shock tube sections are each 6 inches in inside diameter by 40 feet long, and will contain pressures up to 20,000 psi. The nozzle is axially symmetric and is designed for a flow Mach number of 7. When the air speed is changed by changing the stagnation enthalpy level, the nozzle Mach number remains nominally at 7. It is, however, necessary to match the throat area to the total enthalpy by selecting a throat insert appropriate to each air speed.

The light-gas gun shown on the right is an obviously important part of the equipment. It is a deformable piston type (ref. 1), with a launch tube bore diameter of 1/2 inch. Behind the launch tube is located a long compressor or pump tube, in this case 36 feet long by 2-1/4 inches inside diameter, which is initially filled with the propellant gas, hydrogen, at a moderate pressure, for example, 50 psia. At the breech end of the pump tube, there is placed a heavy deformable piston, for example, a polyethylene piston 7 diameters long, and behind the piston, a charge of gunpowder. When the powder is ignited, the piston is driven down the pump tube, to a maximum velocity of about 2,000 ft/sec, compressing the hydrogen ahead of it. When the hydrogen pressure reaches a predetermined value, for example, 20,000 psi, a diaphragm bursts between the pump tube and the model launching tube, and the model is driven down the launch tube by the hot, high-pressure hydrogen. The compressor piston continues to move forward compressing the hydrogen to pressures as high as 200,000 psi during model launch. At the end of its stroke, the piston is driven into a tapered high-pressure coupling, and is deformed by the force of the impact to fit the taper. As was indicated earlier, this gun has been operated above 30,000 ft/sec.

The complete operating cycle of the prototype may now be illustrated by the time-distance diagram in figure 2. The cycle begins at $t = -60$ msec with ignition of the driver gases, which are a mixture of hydrogen, oxygen, and

helium, with nitrogen added to bring about tailoring of the shock tube at the desired stream total enthalpy (ref. 6). As shown at $t = -6$ msec (in this example), the gun cycle is initiated by igniting the gunpowder. At $t = 0$, a diaphragm punch is actuated to pierce and commence opening the principal diaphragm located between the shock tube and driver at $x = 40$ feet. The shock wave and interface then move down the shock tube at high velocity, compressing the supply air for the wind-tunnel operation. With a flow velocity in the test section of 12,000 ft/sec, and the present nozzle throat which gives a flow Mach number of 7.32, the theoretical time for the compressed air to be expended in flow through the throat is 18.8 msec. Flow in the test section is initiated by a starting shock wave which is an extension in time and position of the path of the principal shock wave in the shock tube. A flow starting period follows during which the air originally in the test section is swept out and the static pressure builds up to the design operating level. By the time flow has started at the downstream end of the test section, the gun cycle has terminated in a model launch which brings the model to the test section at a predetermined speed of from 15,000 to 30,000 ft/sec (the track shown is for 20,000 ft/sec). The model moves through the test section and leaves approximately 5 msec before the period of relatively steady flow is terminated by the arrival of the head of the expansion wave from the shock tube. About 1 msec after the expansion wave arrives, the flow is definitely terminated by the exhaustion of test air, and driver gases enter the test section. The 6 msec excess in the run time shown is, of course, useful because the driver gases tend to enter the test section earlier than predicted, due to interface mixing, and some leeway is needed to insure coordination of the model flight and shock-tube operation. Normally, the timing is planned to bring the model into the test section as soon as flow is established, since it has not yet been definitively established when driver gas

contamination begins. Hence, the earliest possible flight is preferred to avoid contaminated gas flow. The operation of the gun and the shock tube can be successfully coordinated because the cycle times of both are repeatable within about 1 msec. No serious difficulty in achieving coordinated operation has been experienced.

The equipment is shown in figure 3. In figure 3(a) the shock-tube driver is in the background, open at the diaphragm station, with the shock tube in the foreground. The punch mechanism can be seen in the open driver as well as a preformed diaphragm ready for installation. Figure 3(b) is a general view of the model launching gun, with the rectangular launch tube clamp in the foreground, the high pressure coupling beyond it, and the pump or compressor tube in the background. A pump piston and a model are placed on the launch tube in the foreground. Figure 3(c) is a general view of the test section, taken from a position alongside the nozzle, showing the shadowgraph optical components for the 11 stations on the side and above the tunnel, and the vacuum dump tank in the far background. The gun room lies beyond this, through the open door.

Operating Range

The range of test conditions attainable with this equipment are shown in figure 4 in terms of resultant or total test velocity and density in ratio to sea level ambient density. Two regions are shown: that which has been demonstrated to date, and the further extension which is believed to be attainable without major revisions to the equipment or major breakthroughs in technique. The range extends from 0.0002 to about 1/6 of atmospheric density. The maximum velocity demonstrated is 41,000 ft/sec which may be extended to about 47,000 ft/sec with present equipment at peak operation. It will be noted that of the total test velocity at maximum performance, about 30 percent is contributed by the shock-tube wind tunnel and 70 percent by the launch gun. This logically raises

two questions: (1) Can the air velocity be increased? (2) If not, is it worth the effort to develop and operate the complete facility as opposed to the alternative of working with the light-gas gun alone? To answer the second question first, we feel that it is worth the effort, for, while the percentage increase in maximum speed is not great, there are excellent reasons for wanting to perform tests at speeds between 30,000 and 50,000 ft/sec which cannot be reached with the gun alone. Among these, a prominent one is the fact that radiative heating problems of entry bodies do not become really significant for entry into the earth's atmosphere until speeds above the escape speed are reached. Similarly, ionization effects become appreciable only at the higher speeds. Couple this with the fact that the speed range above 36,000 ft/sec is the range required for lunar and planetary missions, unattainable by the gun alone, and it will be seen that the shock-tube wind tunnel's contribution is needed. It should also be realized that the maximum performance of the gun cannot be attained with any but the lightest and most rugged models. For models limited to lower launching velocity, the contribution of the air speed becomes of great importance. Consider, for example, a model that can be launched to only 15,000 ft/sec. By adding the flow of the shock-tube wind tunnel, we can test it to twice that speed.

Concerning the first question, the air velocity can surely be increased but only by lowering the maximum density of the stream. This is shown in figure 4 by the two lower lobes of the solid line boundary on the right, which represent the highest densities attainable at the two highest air speeds (9,000 and 12,000 ft/sec) in current use. Lowering of the density has a number of consequences, one of which is that aerodynamic force and stability tests become less feasible and finally, for any model scale and design, unfeasible at some value of density. Gaseous radiation tests remain possible at lower values. Another

problem with extremely low test densities, which is at present only partly understood, is the occurrence of nonequilibrium conditions in the test stream. Nevertheless, we will make some efforts in our future work to achieve higher air velocities, perhaps up to 20,000 ft/sec.

For aerodynamic tests, the Reynolds numbers implicit in figure 4 are of interest. Typical values based on free-stream conditions and 1/2-inch model diameter for the three corner points on the right-hand boundary of the demonstrated operating range are, from top to bottom, 2,500,000, 350,000, and 74,000. Thus, another disadvantage of increasing the air speed appears - inability to simulate flight Reynolds numbers at the highest air speeds.

Operating Problems

Almost exclusively, the current operating problems with this equipment are associated with the shock-tube wind tunnel. Operating problems with the gun have been largely brought under control, although model launching problems are a continuing feature of this kind of work (for example, inability to separate the sabot without causing major angular or linear disturbance to the model motion, or structural failure of the model or sabot during launch). Other problems with the gun have included recurrent plastic failure in the vicinity of the high-pressure coupling, which has been eliminated by improving the design, and rapid wear of the launch tube, which has been controlled by use of a launch tube with a replaceable liner.

The shock-tube wind-tunnel problems may be classified as combustion problems in the driver, deviations from ideal performance of the shock tube, and calibration and flow steadiness problems in the test section. The combustion problems have centered around the difficulty of obtaining uniform mixture of the propellant gases throughout the 40 feet of combustion chamber and of

achieving a uniform rate of pressure rise at all stations of the chamber. When this is not achieved, long-wavelength pressure oscillations form, sloshing from end to end of the tube at the speed of sound. Such a condition is shown by an oscillograph trace in figure 5. The slosh waves obey the prediction of the classical theory of strong sound waves and develop into shock waves (shown by the vertical pressure rise) after completing about two oscillations. Altering the gas loading procedure to introduce about three fourths of the helium after all of the combustible gases were loaded resulted in the smooth burning behavior shown by the traces on the right. Although the order of loading the gases cannot be arbitrary, for safety reasons, no difficulty has been experienced with the current procedure of loading the oxygen and nitrogen first, then adding one fourth of the helium, then all of the hydrogen, and finally the remainder of the helium. The gases are ignited by pulse heating an axial tungsten wire, which is heated in a period of microseconds to a bright glowing condition by a condenser discharge. This technique was shown in preliminary small-scale tests to be less likely to initiate detonation than was the use of exploding wire ignitors. Driver gas detonation has not occurred except in two or three instances where the ignition wire broke before the ignition pulse was applied. This resulted in flame path lengths greater than critical and, consequently, detonation. With the current practice of checking the continuity of the ignition wire just prior to ignition, no problems with detonation are experienced.

Nonideal operation of the shock tube results from several causes including the finite opening time of the principal diaphragm, the formation of a boundary layer in the gases running down the tube, the mixing of the driver and driven gases at the interface, and a nonplanar reflection surface at the shock reflection station which is also the entrance to the nozzle. Respectively, these result in

an initial period of formation of the normal shock wave, the subsequent attenuation of the wave velocity as it runs down the tube, a reduction of run time and a complication of the tailoring requirements due to the lack of a sharp interface, and a more complicated shock reflection process involving configurations such as lambda shock waves in place of simple normal shock waves. This latter point is illustrated at the left in figure 6, which is a pressure record obtained at the shock reflection station in a case where the shock tube was terminated by closing the end with a flat plate. At least three distinct pressure jumps steep enough to characterize shock waves were recorded where only two are expected in a simple shock reflection process under conditions suitable for tailored operation. The steadiness of the pressure after the reflection process is complete suggests that tailored operation was, indeed, achieved. Although one can postulate a lambda shock wave model for this process, it does not seem satisfactory in all respects. The net effect of the nonideal shock tube performance is to reduce the steadiness of the test section flow, and shorten the usable run time.

The calibration problem is to define the velocity of flow and the stream density as a function of time and position in the test section, and to detect the onset of contamination by driver gases. The methods of doing this have been indirect. The stream total enthalpy is calculated from measurements of the incident shock velocity in the shock tube and from measurements of the reflection process. The test-section velocity, density, and all other properties may then be computed as a function of time from measurements of static pressure at various stations of the test section, assuming isentropic flow. Redundant measurements of pitot pressure and Mach number (from shock-wave angle on a stationary cone) have generally confirmed the validity of this approach, although a question of precision arises. It is believed that present density determinations are accurate to no better than 10 percent, and a more direct determination of density is

considered a future goal. Better definition of the onset of driver gas contamination is also desired; information on this is fragmentary so far, having been obtained from a variety of observations such as standoff distance of the bow shock wave of a blunt model, and should be studied in a more systematic fashion.

The steadiness of flow during the running period is far from perfect. This is shown by the static pressure traces to the right in figure 6, obtained near the two end stations of the test section. (Note that these are not from the same test as the stagnation pressure record shown.) To what extent the unsteadiness is due to disturbances originating in the shock tube, and to what extent due to boundary-layer growth and other boundary-layer disturbances in the test section cannot be stated at present. It is possible, for example, that the short-period oscillations are attributable to an unsteady turbulent boundary layer on the walls of the test section. Spikes can be seen on the record corresponding to the time the model bow wave intersects the pressure cells. This provides a signal from which the value of static pressure in the station at the time the model was there can be deduced.

The above problems are, it is believed, common to all shock-tube and shock-tube wind-tunnel systems. They are not prohibitive in the sense that they do not prevent useful measurements with these devices. They do, however, adversely affect the precision of measurements. The loss of precision depends, of course, on the kind of measurement. It is to be expected that as time goes by, our understanding of the causes of some of these operating difficulties will improve, as will the smoothness of the operation (see, e.g., the reduction in the magnitude of the slosh waves).

OBSERVATIONS FROM SOME OF THE EARLY RESEARCH PROGRAMS

A major part of the research effort in these facilities to date has been concerned with measurements of air radiation behind the bow waves of bodies

traveling at speeds up to 44,000 ft/sec. The results have been published in references 3, 4, and 5, and will not be described here in any detail. These measurements have contributed to the definition of both equilibrium and nonequilibrium radiative heating of entry bodies. Figure 7 taken from reference 5 shows the data for equilibrium-dominated conditions for the speed range from 18,000 to 41,000 ft/sec. The form in which the data are plotted makes them applicable to vehicles of all scales at all altitudes at which flow equilibrium is attained. General agreement with the theoretical curves is found; but the scatter in the experimental data is appreciable at the higher speeds, and further work will be necessary to reduce it. Generally speaking, however, we may say that the magnitude of equilibrium radiation is now established for this speed range. The same may be said of the nonequilibrium radiation on the basis of experimental information shown in figure 8, also from reference 5. Here the nonequilibrium radiation per square centimeter of shock-wave surface is shown as a function of the velocity normal to the shock wave. The magnitude of this radiation is small compared to what was predicted theoretically a year or two ago, but the agreement of data obtained by the considerably different techniques of shock tube and free-flight facilities is evidence that no major experimental errors are present. The nonequilibrium radiation is expected to be of the magnitude shown or, at very high altitudes, smaller, because of flow energy limitation, truncation of the nonequilibrium region by the flow expansion, and a number of other limiting effects.

Many of the interesting phenomena encountered in research with these facilities have been a result of interaction of the materials of the test model with the hypervelocity air flow. At the speeds and air densities covered, model ablation generally takes place. In fact, to avoid ablation, it is necessary to calculate carefully from the heat sink properties of the model the limitations

on speed and density which must not be exceeded. Aluminum models with pointed tips are especially vulnerable to ablation, since aluminum is a very poor ablation shield material. The fact that it melts at relatively low temperature and burns in air leads to some rather spectacular effects when aluminum models are used. The shape change of an aluminum cone in 40 feet of flight in air at 0.01 of atmospheric density at a speed of 32,000 ft/sec is illustrated in figure 9. The two pictures on the left show a 30° half-angle cone, initially sharp. The sabot halves may be seen just separating from the model at the first station, labeled $t = 0$; 1.25 msec later, an appreciable rounding of the tip has occurred. On the right, an initially round-nosed cone with tip radius of one third the base radius is shown, and its nose is noticeably flattened by ablation during the flight. The onset of aluminum ablation is accompanied by a flare of luminosity which is particularly observable with conical models for which the air radiation is very low. For ablating aluminum cones, luminosity has been observed to be as much as 1,000 times greater than the radiation produced by the shock-layer air.

Radiation effects are, in fact, quite generally associated with products of ablation in the flow field. A further example of this is shown in figure 10 which is a sequence of three photographs of an ablating polyethylene model as it progresses across the field of view of an image converter camera. The intervals between pictures were 2 and 5 microseconds, and the exposure times were 1/5 microsecond. While the luminosity on the model face is partly due to air in the shock layer, that in the wake originates almost entirely from ablation products. This has been demonstrated experimentally by changing the materials of which the models are made, and, under selected conditions, by use of aluminum models at conditions below which ablation does not occur. In the latter case, the level of radiation from the wake is at least one order of magnitude below that from the shock layer, and if the exposure is set to photograph the shock layer, no luminosity from the wake is recorded.

The wake luminosity is useful as a flow visualization aid in these pictures. It shows the region of the wake which is laminar, and shows the pattern of breakdown into turbulence. Turbulence begins in this case at 3 to 4 body diameters behind the base, corresponding to 2 to 3 diameters behind the minimum section of the wake. In the bottom picture, a clearly defined helical pattern of wake flow is established, with a helix angle of $45^{\circ} \pm 5^{\circ}$. In addition, some large lumps of turbulence develop, and act to transport luminous ablation product material into the outer flow, as may be seen from the haze of luminosity which develops outside the bright center portion.

Luminosity of ablation products is not confined to the wake region, however, since it appears as well in the radiation from the shock layer, as shown by quantitative measurements of Craig and Davy in figure 11. The four parts of this figure show low-resolution spectra obtained in the wavelength region from the ultraviolet to the near infrared from the shock layer of models of four materials, aluminum (below the ablation temperature), and three plastics, polyethylene, G. E. 124, and lexan (a polycarbonate). These spectra were obtained at approximately the same speed in free-stream air of 0.02 atmospheric density. The observed radiation power is normalized to the effective volume of the shock layer, as though the luminosity were uniformly distributed, although this is clearly not correct for any radiation originating in the ablation products. However, for comparative purposes, it is a satisfactory presentation. It shows that large differences in the shock-layer radiation spectrum result from changes in model material. The largest effect is the additional radiation peaking at about 0.7 micron, most pronounced with the polycarbonate model. A progression of radiation intensity in this wavelength region is evident in progressing from nonablating aluminum through polyethylene and G. E. 124 to the polycarbonate. A theoretical estimate of the radiation to be expected from the air in the shock

layer at equilibrium is included for these test conditions in the upper left spectrum. It has only a very small contribution in the infrared. It does not agree well with experiment at the ultraviolet end of the spectrum at this air density, but this is a result of the presence in significant amounts of non-equilibrium air radiation. At higher air densities, the theory and the aluminum model spectrum come into closer agreement.

The significance of ablation product radiation as a source of radiative heat input to entry bodies has been studied from these data. By use of a boundary layer analysis, given in a prospective report by Craig and Davy, scaling rules have been written which indicate that at certain conditions of speed and altitude, ablation product radiation can be a source of considerable heat input, in some cases greater than air radiation, particularly for materials as bad as lexan in this regard.

Since it is observed that there is appreciable ablation product radiation in the shock layer and in the wake, it is interesting to compare spectra from these two regions. For purposes of making this comparison, we subtract the shock-layer air radiation from the observed total shock-layer radiation to obtain the radiation attributable to the presence of ablation products. The shock-layer air radiation is assumed to be given by the test with a nonablating aluminum model. Ablation products spectra from the shock layer, obtained in this way, are compared in figure 12 with wake spectra for two different model materials. Note that comparisons of the absolute levels of radiation are not of direct significance in this figure, since the total radiation of ablation products from the shock layer is compared with the wake radiation from an arbitrary length of wake, approximately equal to 1-1/2 model diameters, at the station of peak wake brightness. However, the spectra may be compared for similarity. In the case of the G. E. 124 material, the similarity is striking, and supports the

view that the wake radiation and the ablation products radiation are from the same source. The principal difference occurs in the ultraviolet, and can perhaps be explained as a result of lower temperatures in the wake than in the gas cap. For lexan, the agreement of the two spectra is less exact, although if we multiply the arbitrary level of the wake spectrum by about 0.6, the correspondence becomes more evident. The dissimilarity at the visible and ultraviolet end of the spectrum is more pronounced in this case than for the other material. Further work should be undertaken in obtaining a detailed description of the chemical processes involved and the radiating species present.

Another materials problem which may prove to be important for space vehicle entries in which the heating rate becomes large compared to present experience is the problem of thermal shock of heat-shield materials. The heating rates will tend to become higher with increasing entry velocity (proportional approximately to V^3) and are also increased by steep entries, such as those considered for unmanned planetary probes. It is not difficult to find combinations of conditions that correspond to peak heating rates in excess of 100,000 Btu/sec ft^2. At some heating rate which is a function of the material, it would be expected that all materials will become subject to spalling due to thermal shock. This phenomenon has been observed, it is believed, in one test in the prototype facility at a combined speed of 40,740 ft/sec and a stream density of 0.002 sea level density. A blunt polyethylene model, which was observed to be smooth in the first shadowgraph stations, became roughened at the later stations as though by loss of relatively large pieces of the face. Since normal ablation processes do not produce this kind of roughening, it is suspected that spalling of this material occurred at this speed. The stagnation point heating rate is calculated to have been about 18,500 Btu/sec ft^2. Since spalling of the heat shield is a kind of

failure of the heat protection system, resulting, at best, in inefficient loss of weight of the shield, this phenomenon will require future study in these facilities.

One of the purposes for which this equipment was designed is the measurement of aerodynamic stability and forces. In our experience to date, however, this subject has not been emphasized as much as gas radiation. Measurements of stability and drag have been undertaken for three kinds of configurations - a blunt capsule, pointed and round-nosed 30° half-angle cones, and a blunt-nosed flare-stabilized body. The test results have shown a general agreement with expectations - there have been no major conflicts with existing theory or previous experiments. It has been learned that models must be made of materials which are efficient heat shields, since large configurational changes associated with appreciable amounts of ablation like that shown in figure 9 cause changes not only in the aerodynamic properties but also in the center of gravity and inertia. Some difficulty has been experienced also in defining the free-stream air density with the necessary precision. Currently the density is obtained from measurements of the static pressure, which is of the order of 0.2 psia, and the limit of accuracy of the static pressure measuring instrument becomes a factor. Other techniques to measure the density more directly will be developed. Also, the density cannot be treated as uniform through the test section, in general, being subject to variations of the order of 20 percent. Otherwise, the application of the prototype facility for these purposes appears to be reasonably similar to earlier experience with the supersonic free-flight wind tunnel (ref. 2). Two motion records from test flights through the prototype are shown in figure 13. The upper one is a velocity plot for a 30° half-angle cone at a speed of about 27,300 ft/sec, M = 32.8. This plot shows that the drag (slope of the line) is well defined by the data. Similarly, in the lower plot, an angular motion,

combined pitch and yaw, is shown for the blunt capsule at a speed of 30,400 ft/sec, M = 35.9. From this motion, which is regular and well defined, information on static and dynamic stability can be extracted. The dynamic stability is sensitive to variations in stream density along the flight path, so that it is expected that techniques of data analysis will have to be developed to allow for the variation in stream density recorded during the test.

Another example of an early application of this equipment is some work performed by Dale Compton and David Cooper to determine convective heating rates for the stagnation region of a body with a spherical nose. The measurement technique was based on the observation that the flight distance to the point where ablation begins is a measure of the heating rate. For aluminum models the onset of ablation can be detected from the appearance of a trail of aluminum vapor or droplets in the wake. This is illustrated by the shadowgraphs reproduced in figure 14, which show the wake region to be clear at early stations, the trail of vapor referred to above appearing at the later stations. The appearance of vapor in the wake is correlated in the figure with the stagnation point surface temperature calculated by the theory of reference 7, with proper allowance for the diffusion of heat inside the model. The flight speed for the test shown is approximately 20,000 ft/sec, below that for which flow ionization becomes significant, and the theory of reference 7 should be applicable. The expected melting temperature of the model is 1270° F, and aluminum vapor is observed to begin to appear in the wake at very near this temperature. Tests at this speed were made to investigate the validity of the measurement technique. Tests at a higher speed of 36,000 ft/sec have been made to establish heating rates for flows with appreciable ionization. The preliminary results are compared with theories and collected data in figure 15 in a presentation adopted from reference 8. The values obtained are shown by the filled symbols. All of the

other data in this figure are from shock tube tests, performed with thin resistance film thermometer instrumentation in testing times of a few microseconds. The free-flight testing time was a few hundred times greater, from 1 to 2 milliseconds, and the instrumentation technique was, as noted, quite different. The data obtained agree with the predominant part of the shock-tube data and fall somewhat below the lowest of the theoretical estimates shown.

CONCLUDING REMARKS

In conclusion, it may be said that the countercurrent facility combining a shock-tube wind tunnel and a light-gas gun has been made to work and is providing laboratory test information in the velocity range of today's highest speed space vehicles. It is not without its problems; however, we believe that these problems will be solved to a degree which will permit the necessary test data to be obtained. It may be remarked that this equipment is capable in principle of providing tests with gases other than air.

Extensions of speed are believed to be not only possible but inevitable. It is difficult to predict the ultimate performance of light-gas guns, but there is no documented reason for believing that the limit has been reached. The acceleration of gas streams to somewhat higher speeds than are currently being used at useful levels of gas density is also possible. It seems reasonable to expect that these techniques will take us into the velocity region between 50,000 and 60,000 ft/sec in the next five years.

REFERENCES

1. Curtis, John S.: An Accelerated Reservoir Light-Gas Gun. NASA TN D-1144, 1962.

2. Seiff, Alvin: A Free-Flight Wind Tunnel for Aerodynamic Testing at Hypersonic Speeds. NACA Rep. 1222, 1955.

3. Page, William A., Canning, Thomas N., Craig, Roger A., and Stephenson, Jack D.: Measurements of Thermal Radiation of Air From the Stagnation Region of Blunt Bodies Traveling at Velocities up to 31,000 Feet Per Second. NASA TM X-508, 1961.

4. Canning, Thomas N., and Page, William A.: Measurements of Radiation From the Flow Fields of Bodies Flying at Speeds up to 13.4 Kilometers Per Second. Paper presented to the Fluid Mechanics Panel of Advisory Group for Aeronautical Research and Development, Brussels, Belgium, April 1962.

5. Page, William A.: Shock-Layer Radiation of Blunt Bodies Traveling at Lunar Return Entry Velocities. IAS Paper 63-41, 1963.

6. Hertzberg, A., Smith, W. E., Glick, H. S., and Squire, W.: Modifications of the Shock Tube for the Generation of Hypersonic Flow. Cornell Aeronautical Laboratory Rept. No. AD-789-A-2, AEDC-TN-55-15 (March 1955).

7. Fay, J. A., and Riddell, F. R.: Theory of Stagnation Point Heat Transfer in Dissociated Air. Jour. Aero. Sci., vol. 25, no. 2, Feb. 1958.

8. Goodwin, Glen, and Howe, John T.: Recent Developments in Mass, Momentum, and Energy Transfer at Hypervelocities. NASA SP-11. NASA-University Conference on Science and Technology of Space Exploration, vol. 2, Chicago, Illinois, Nov. 1-3, 1962. Also available as NASA SP-24, Gas Dynamics in Space Exploration, Dec. 1962.

SCHEMATIC DRAWING OF THE PROTOTYPE FACILITY

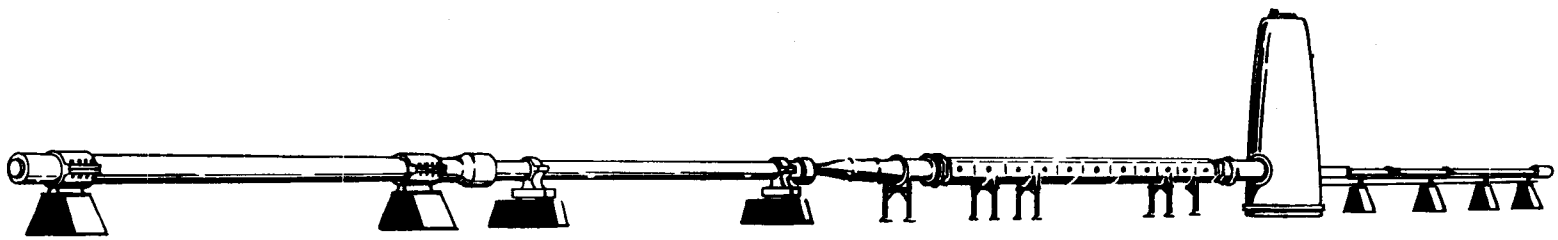

Figure 1

NATIONAL AERONAUTICS AND SPACE ADMINISTRATION
AMES RESEARCH CENTER, MOFFETT FIELD, CALIFORNIA

OPERATING CYCLE OF PROTOTYPE FACILITY

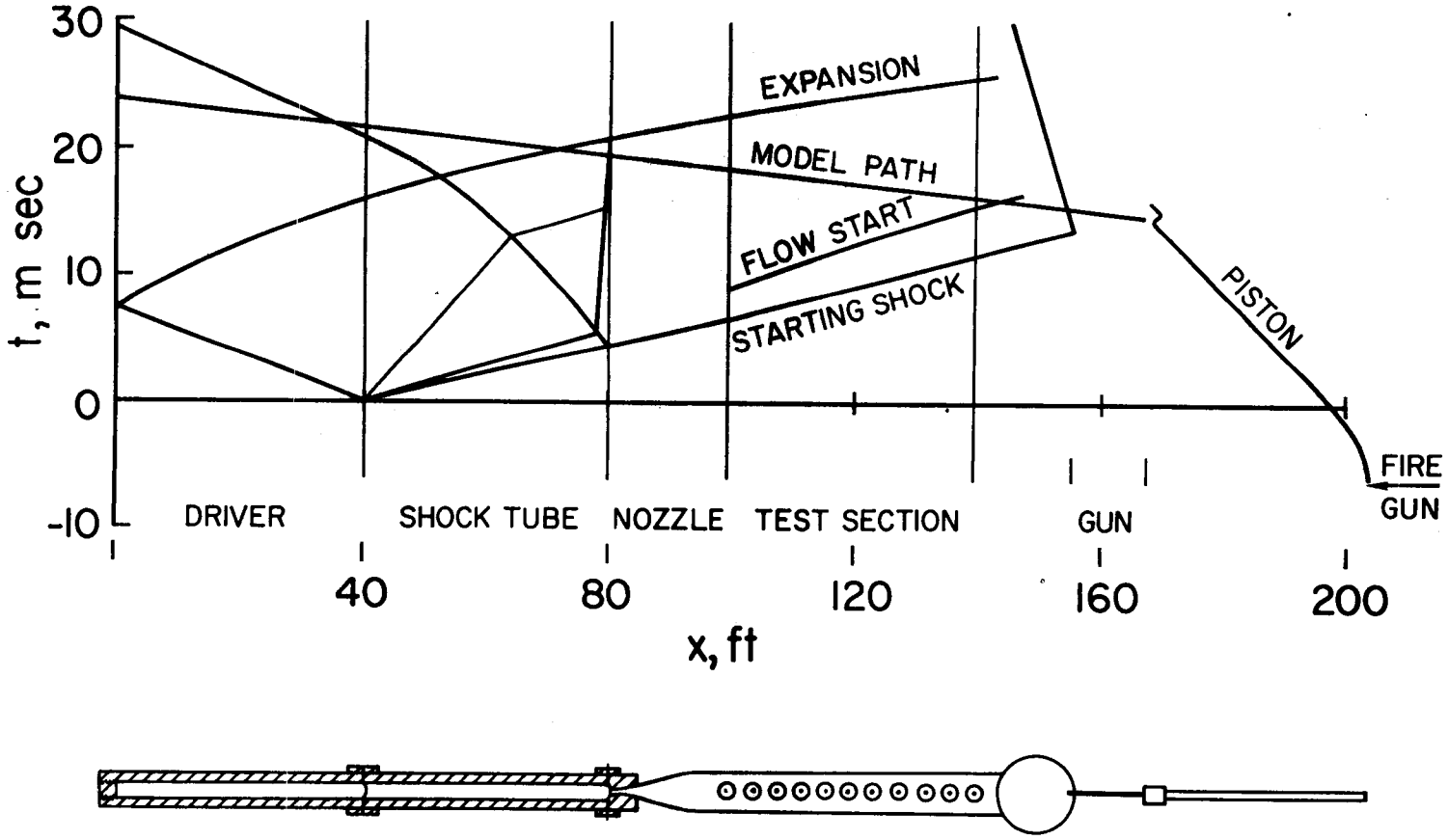

Figure 2

NATIONAL AERONAUTICS AND SPACE ADMINISTRATION
AMES RESEARCH CENTER, MOFFETT FIELD, CALIFORNIA

GENERAL VIEWS OF PROTOTYPE FACILITY
SHOCK TUBE

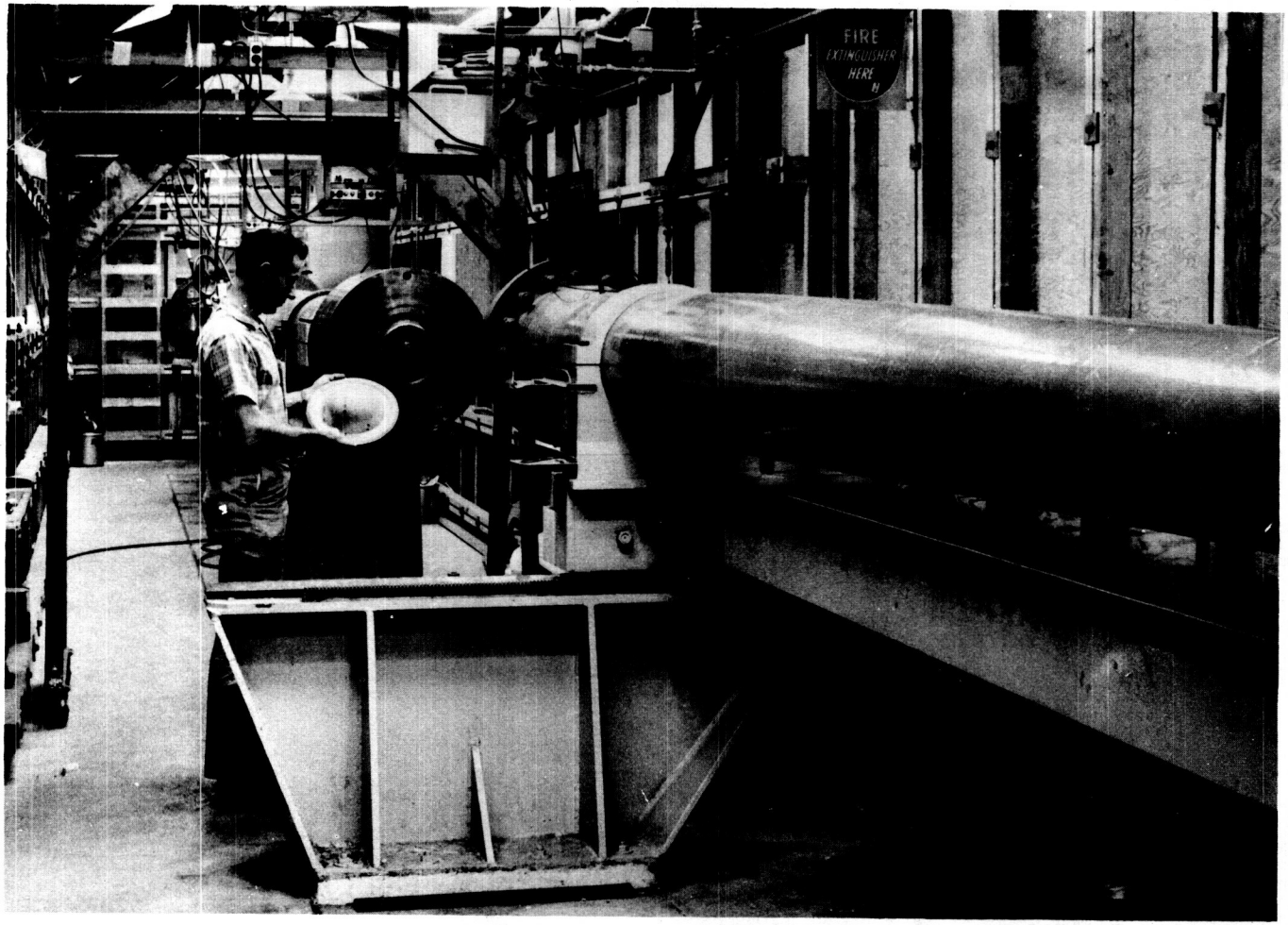

A-30556

Figure 3(a)

NATIONAL AERONAUTICS AND SPACE ADMINISTRATION
AMES RESEARCH CENTER, MOFFETT FIELD, CALIFORNIA

GENERAL VIEWS OF PROTOTYPE FACILITY
LIGHT GAS GUN

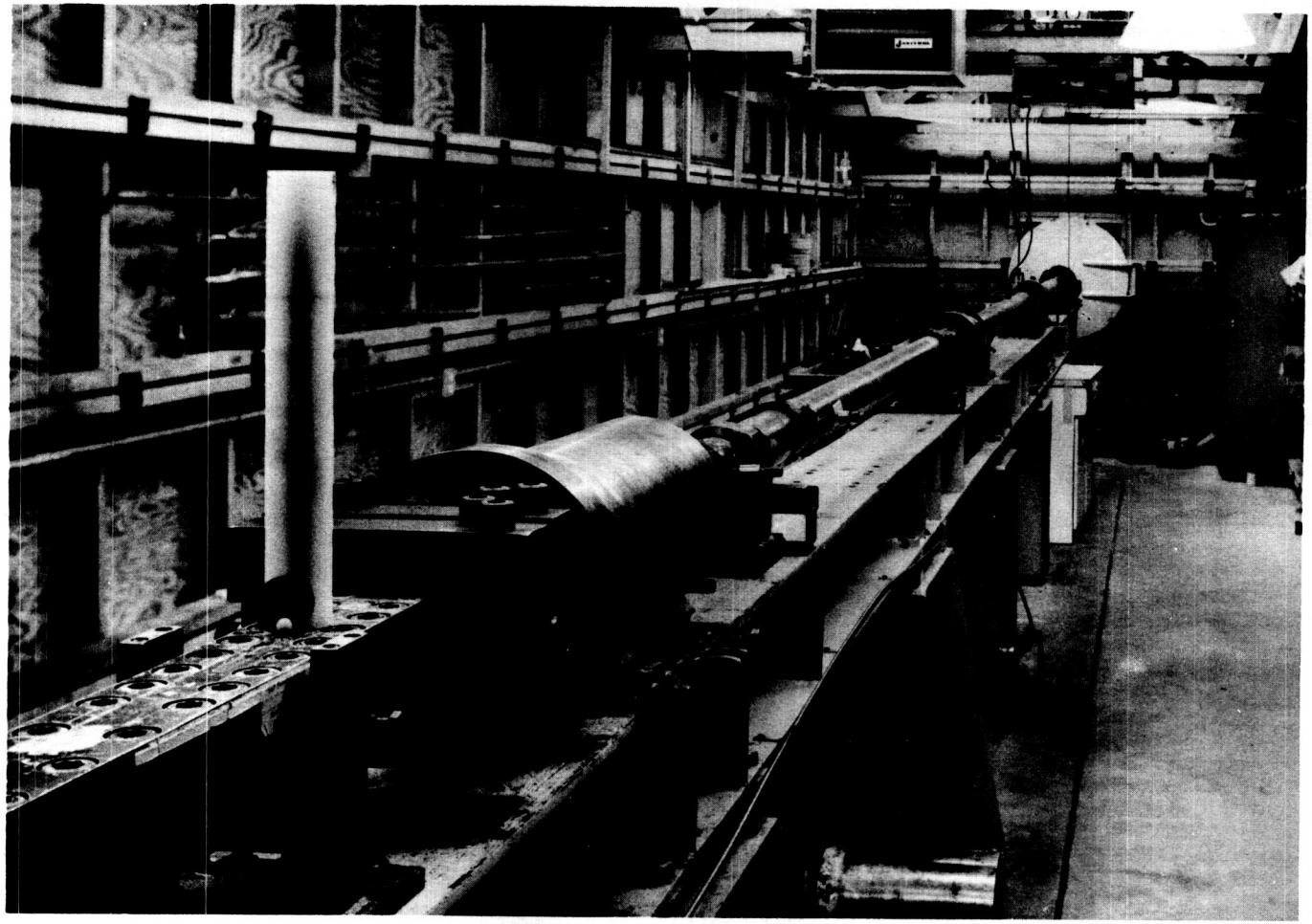

A-30558

Figure 3(b)

NATIONAL AERONAUTICS AND SPACE ADMINISTRATION
AMES RESEARCH CENTER, MOFFETT FIELD, CALIFORNIA

GENERAL VIEWS OF PROTOTYPE FACILITY
TEST SECTION

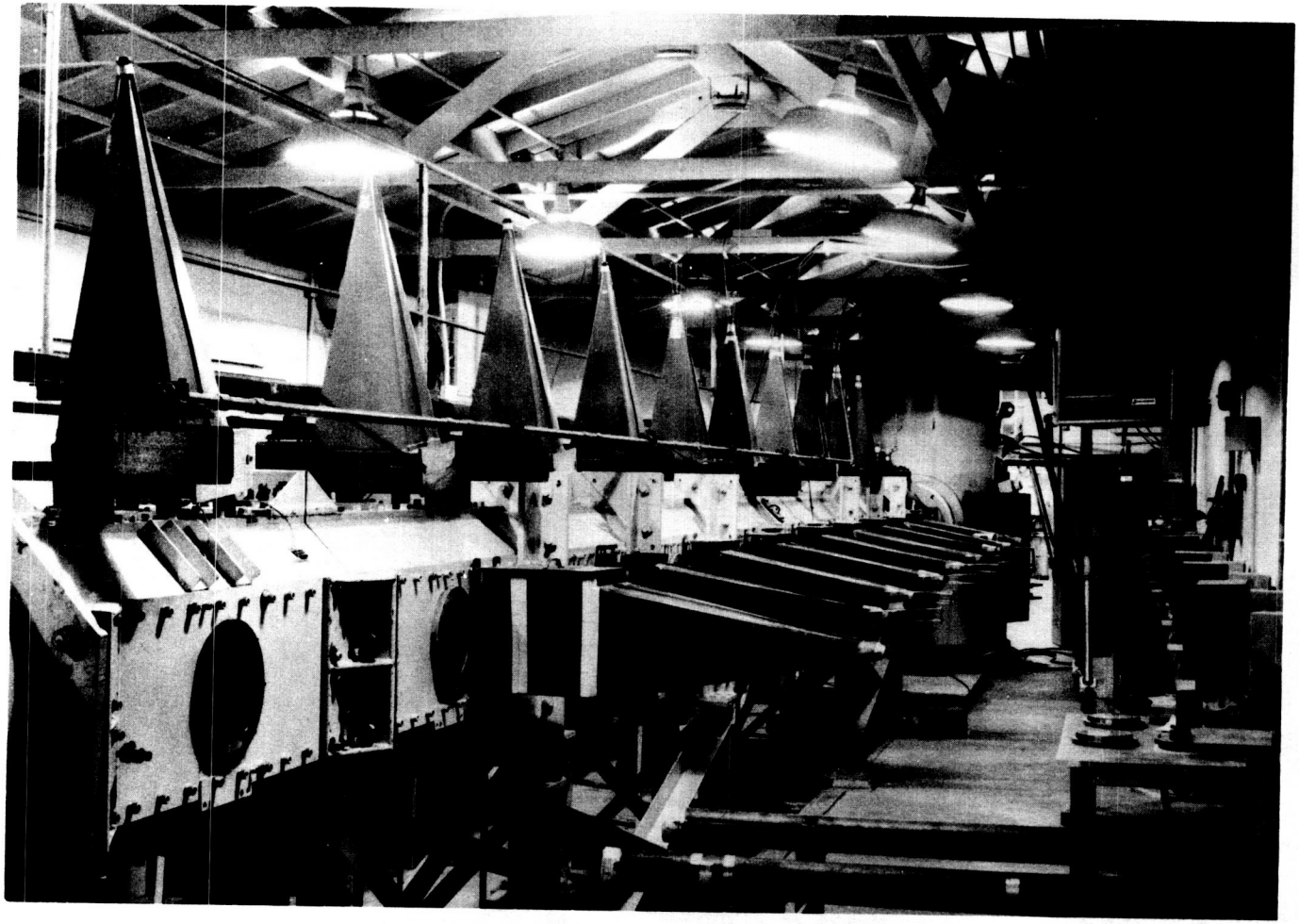

A-30557

Figure 3(c)

NATIONAL AERONAUTICS AND SPACE ADMINISTRATION
AMES RESEARCH CENTER, MOFFETT FIELD, CALIFORNIA

VELOCITY AND FREE-STREAM DENSITY RANGE OF PRESENT EQUIPMENT

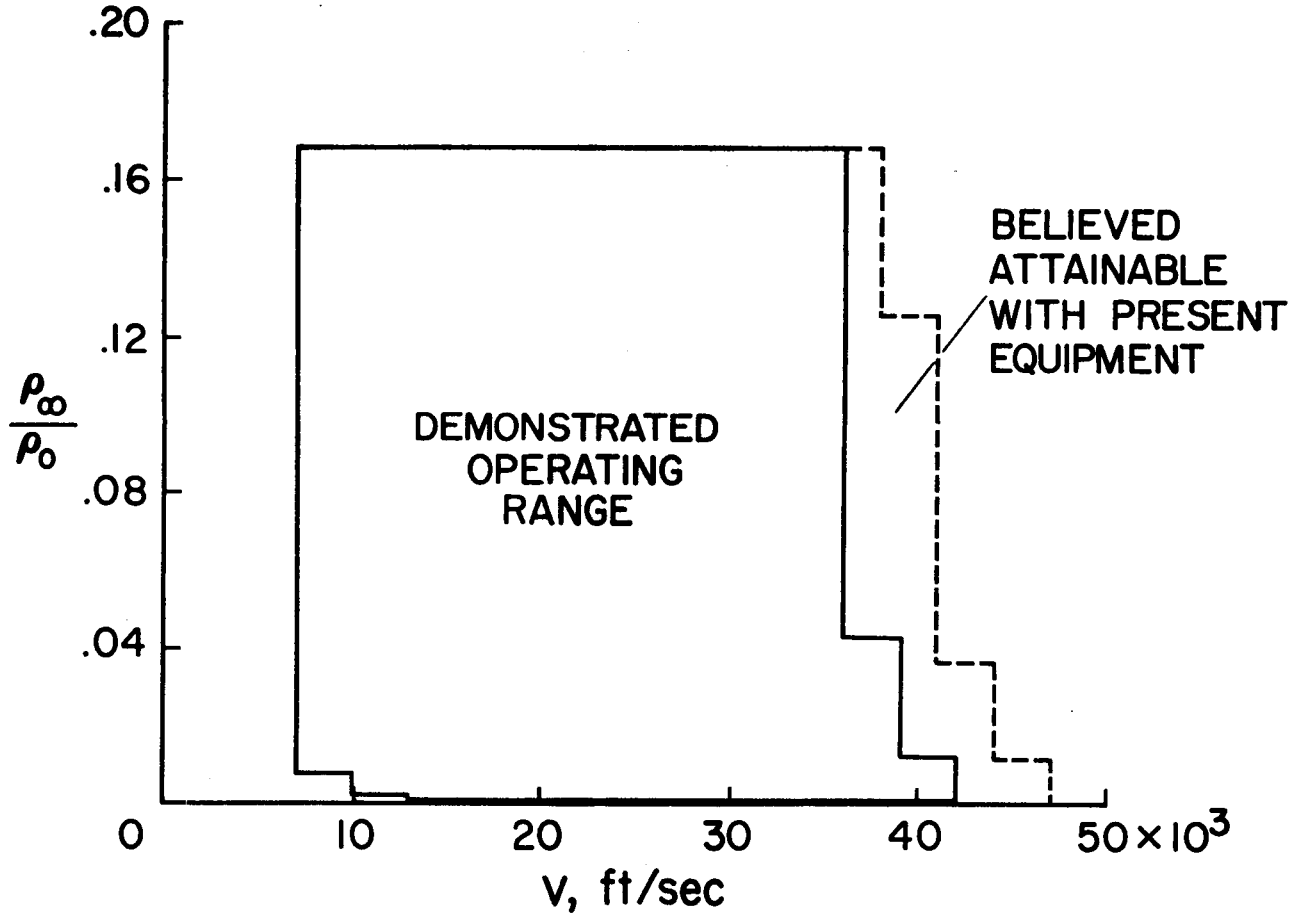

Figure 4

NATIONAL AERONAUTICS AND SPACE ADMINISTRATION
AMES RESEARCH CENTER, MOFFETT FIELD, CALIFORNIA

COMBUSTION CHAMBER PRESSURE RECORDS

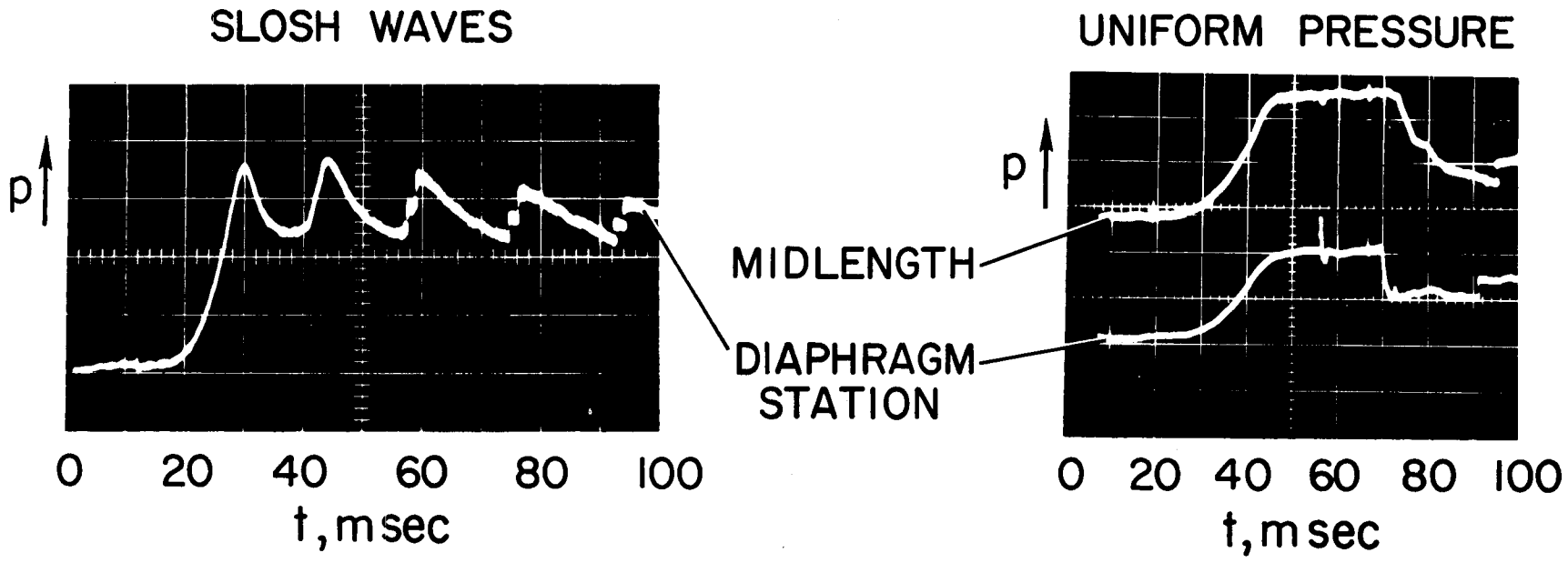

Figure 5

NATIONAL AERONAUTICS AND SPACE ADMINISTRATION
AMES RESEARCH CENTER, MOFFETT FIELD, CALIFORNIA

FLOW STAGNATION AND STATIC PRESSURE RECORDS

STAGNATION PRESSURE IN SHOCK TUBE

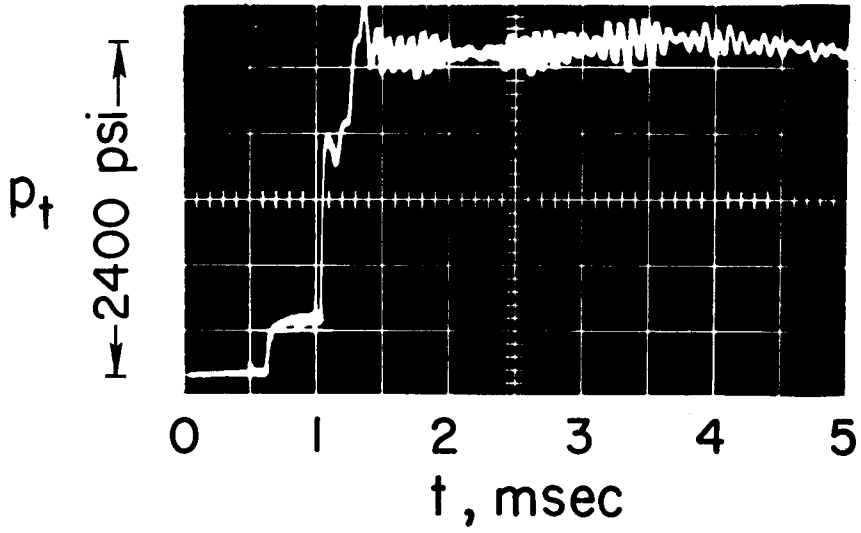

STATIC PRESSURE IN TEST SECTION

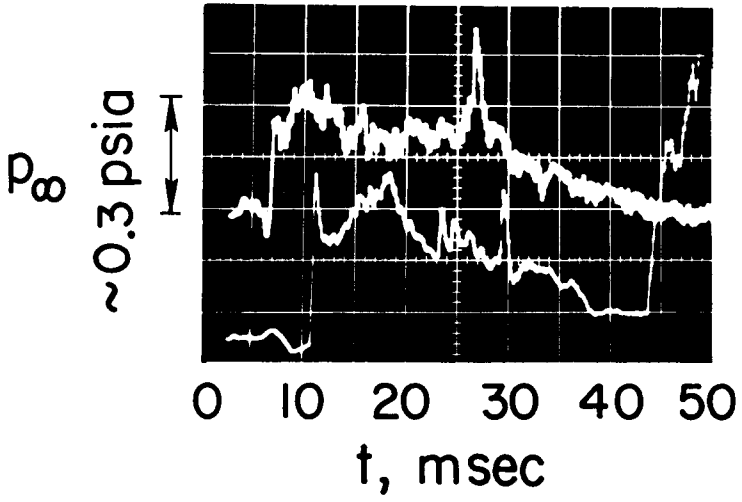

Figure 6

NATIONAL AERONAUTICS AND SPACE ADMINISTRATION
AMES RESEARCH CENTER, MOFFETT FIELD, CALIFORNIA

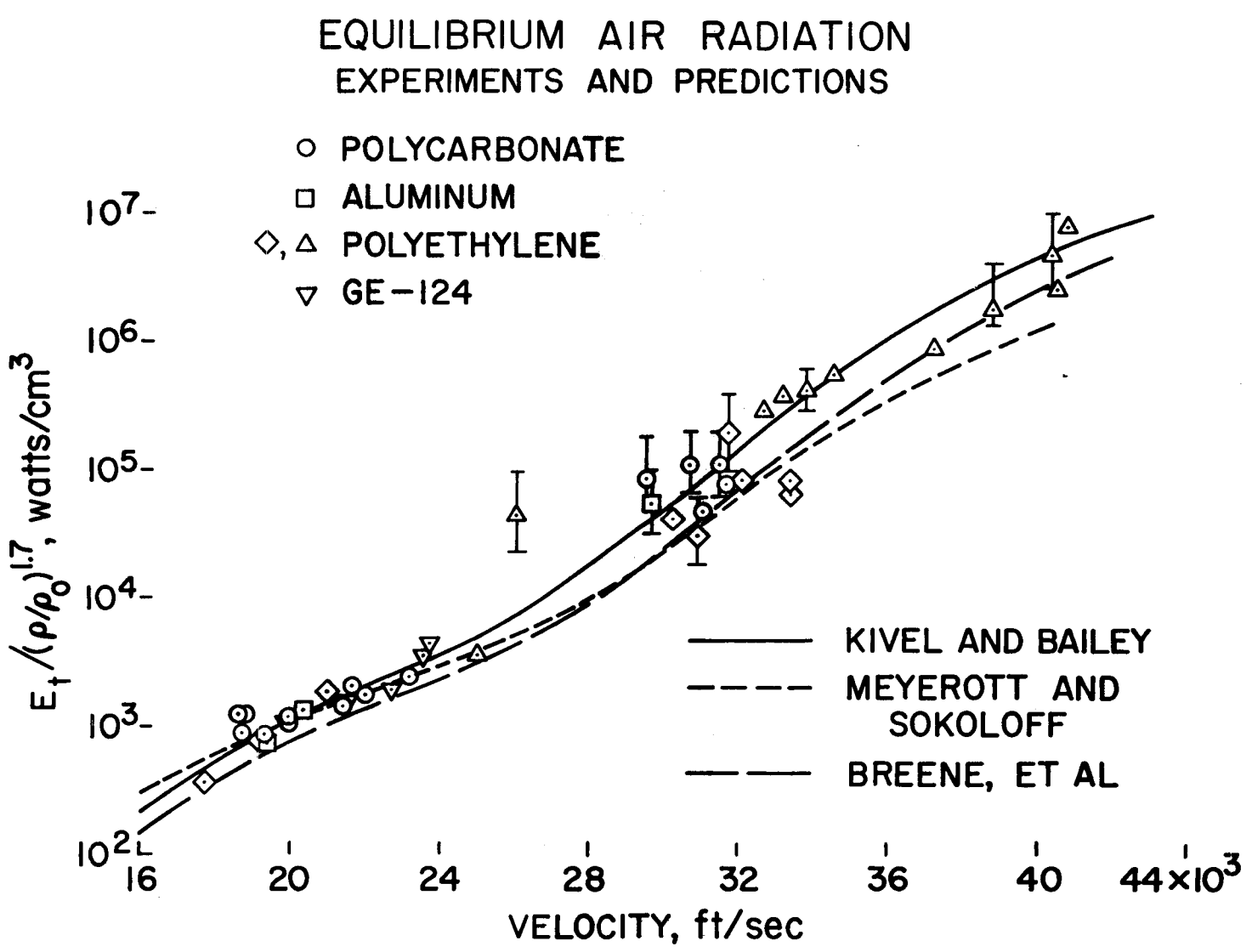

Figure 7

NATIONAL AERONAUTICS AND SPACE ADMINISTRATION
AMES RESEARCH CENTER, MOFFETT FIELD, CALIFORNIA

MEASUREMENTS OF NONEQUILIBRIUM AIR RADIATION

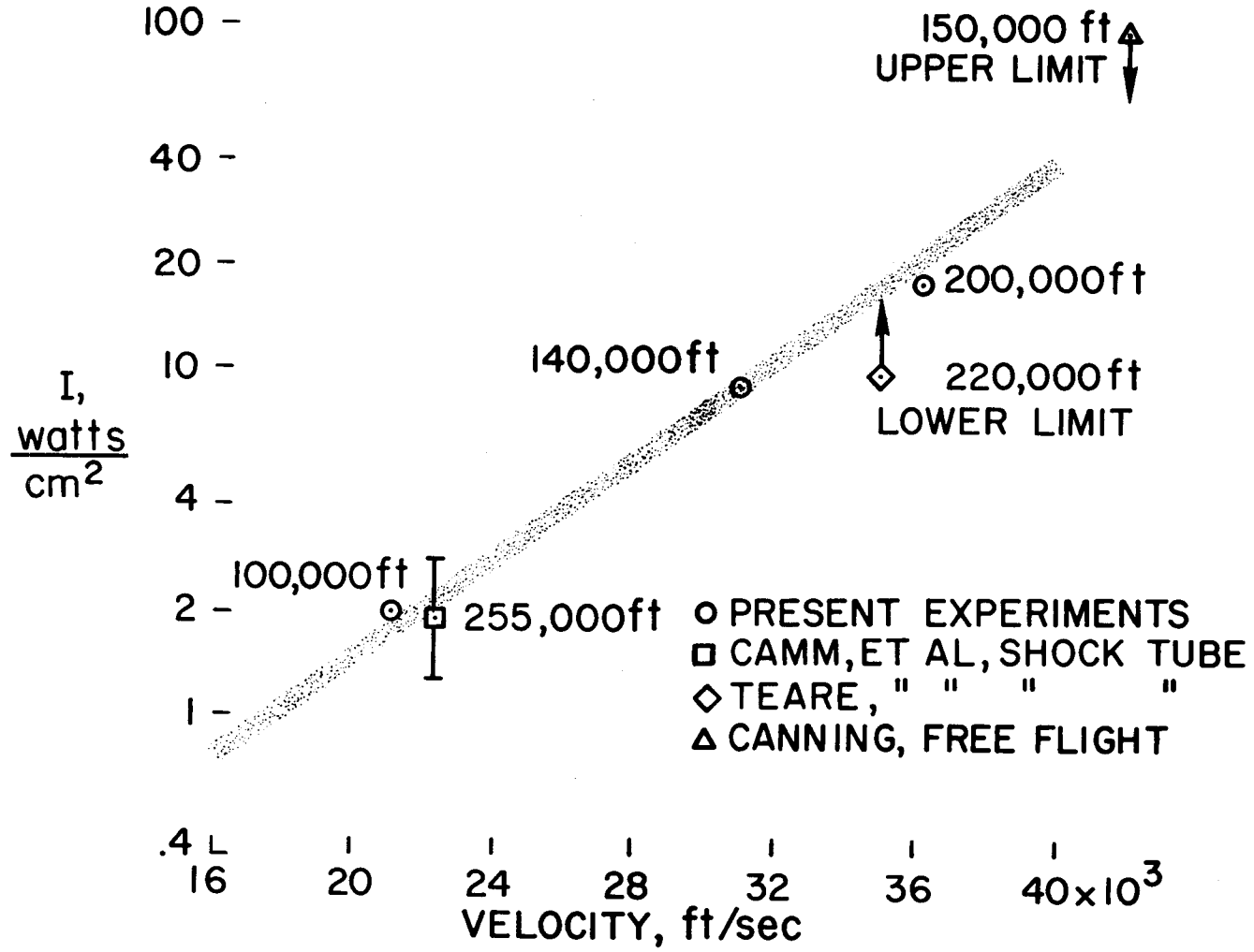

Figure 8

NATIONAL AERONAUTICS AND SPACE ADMINISTRATION
AMES RESEARCH CENTER, MOFFETT FIELD, CALIFORNIA

SHADOWGRAPHS SHOWING TIP ABLATION ON ALUMINUM CONES AT V = 32,000 ft/sec, $\rho_\infty/\rho_0 = .01$

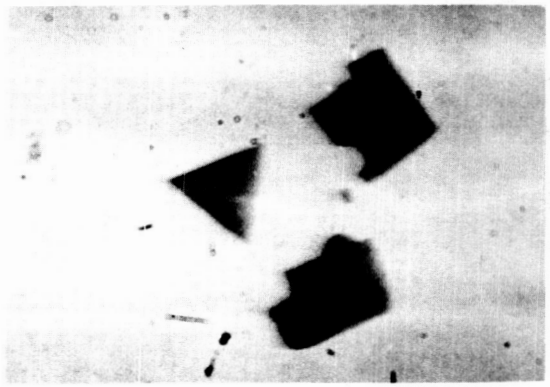

t = 0

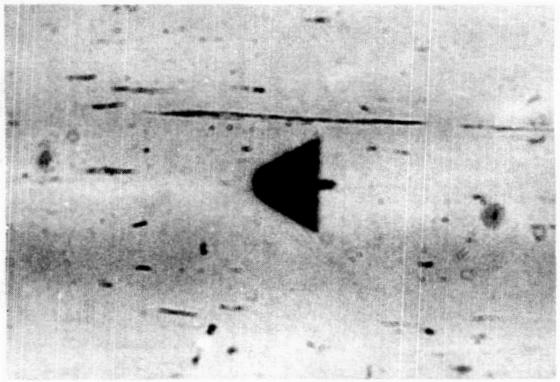

t = 0

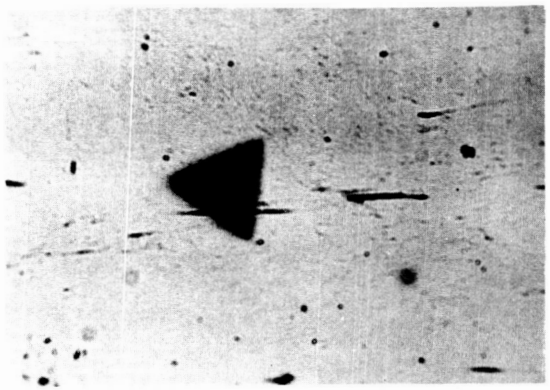

t = 1.25 msec

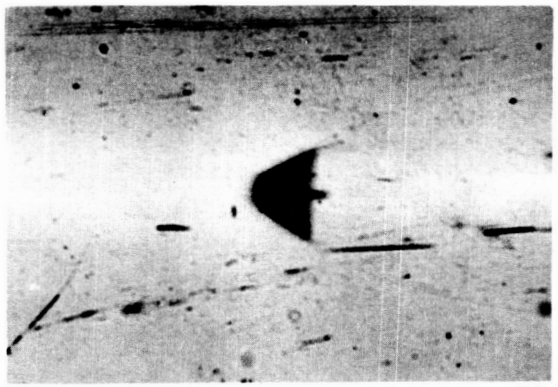

t = 1.25 msec

A-30646

Figure 9

NATIONAL AERONAUTICS AND SPACE ADMINISTRATION
AMES RESEARCH CENTER, MOFFETT FIELD, CALIFORNIA

LUMINOUS WAKE WITH TRANSITION TO TURBULENCE

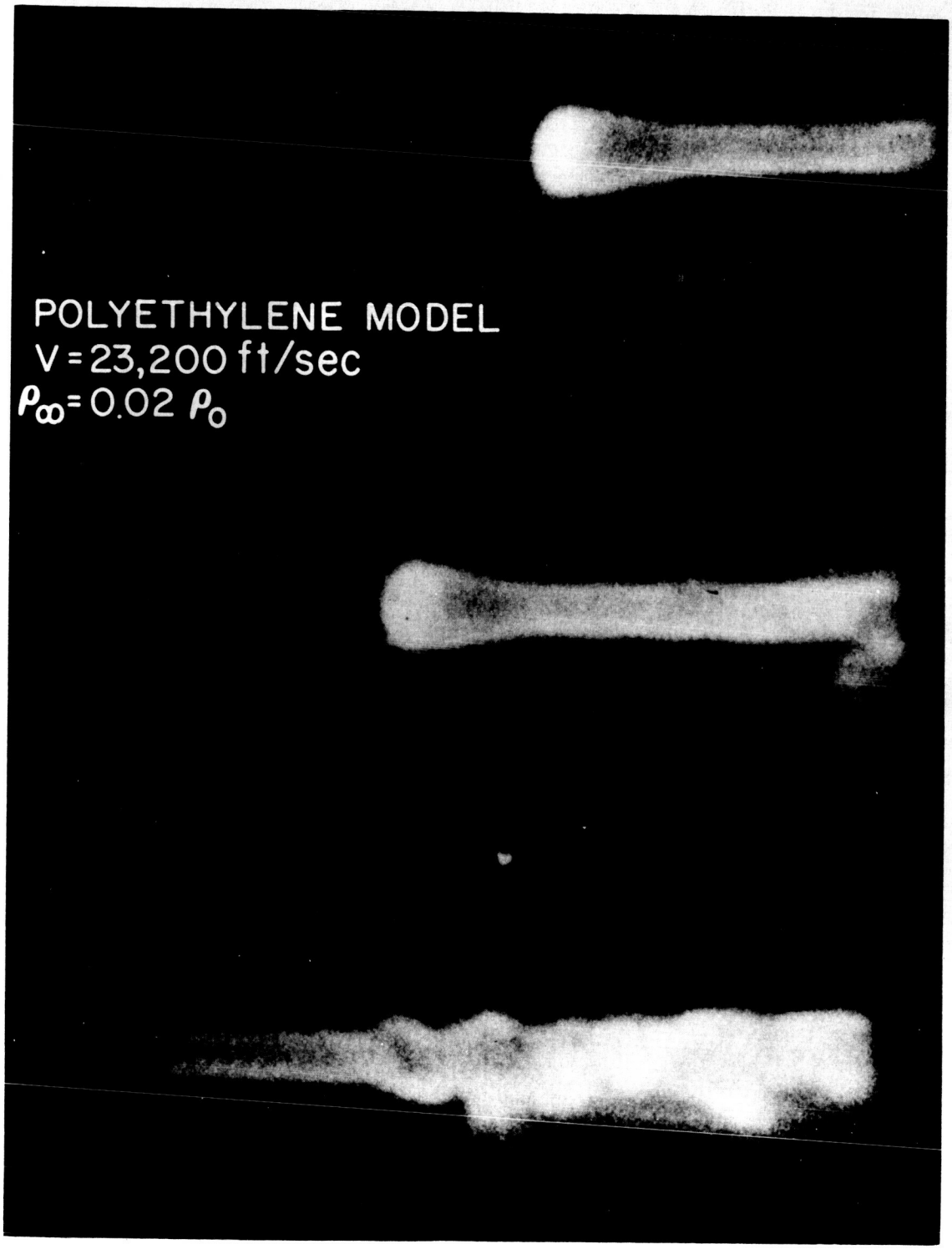

A-30235.1

Figure 10

NATIONAL AERONAUTICS AND SPACE ADMINISTRATION
AMES RESEARCH CENTER, MOFFETT FIELD, CALIFORNIA

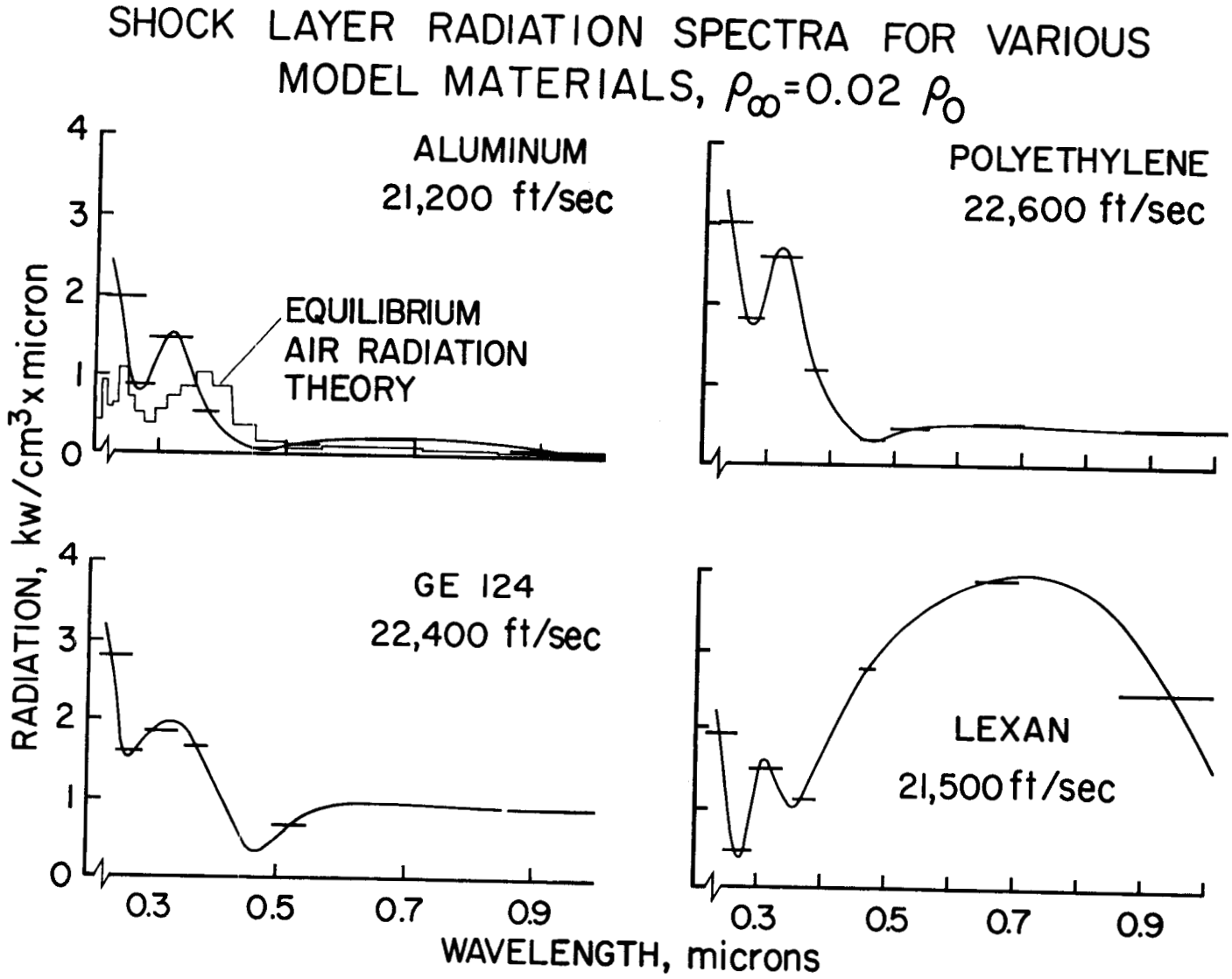

Figure 11

NATIONAL AERONAUTICS AND SPACE ADMINISTRATION
AMES RESEARCH CENTER, MOFFETT FIELD, CALIFORNIA

SPECTRA OF ABLATION PRODUCTS RADIATION IN WAKE AND SHOCK LAYER

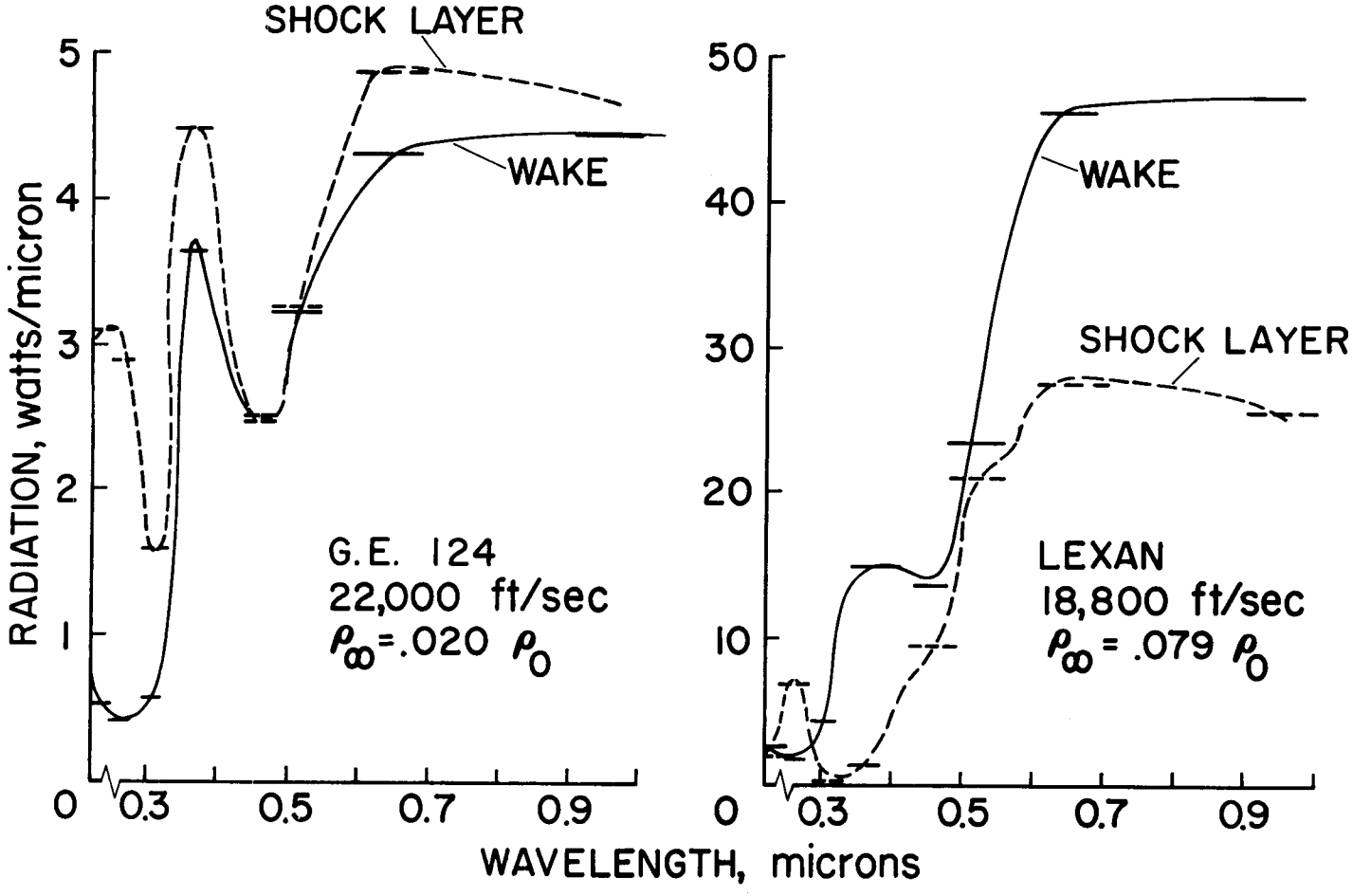

Figure 12

NATIONAL AERONAUTICS AND SPACE ADMINISTRATION
AMES RESEARCH CENTER, MOFFETT FIELD, CALIFORNIA

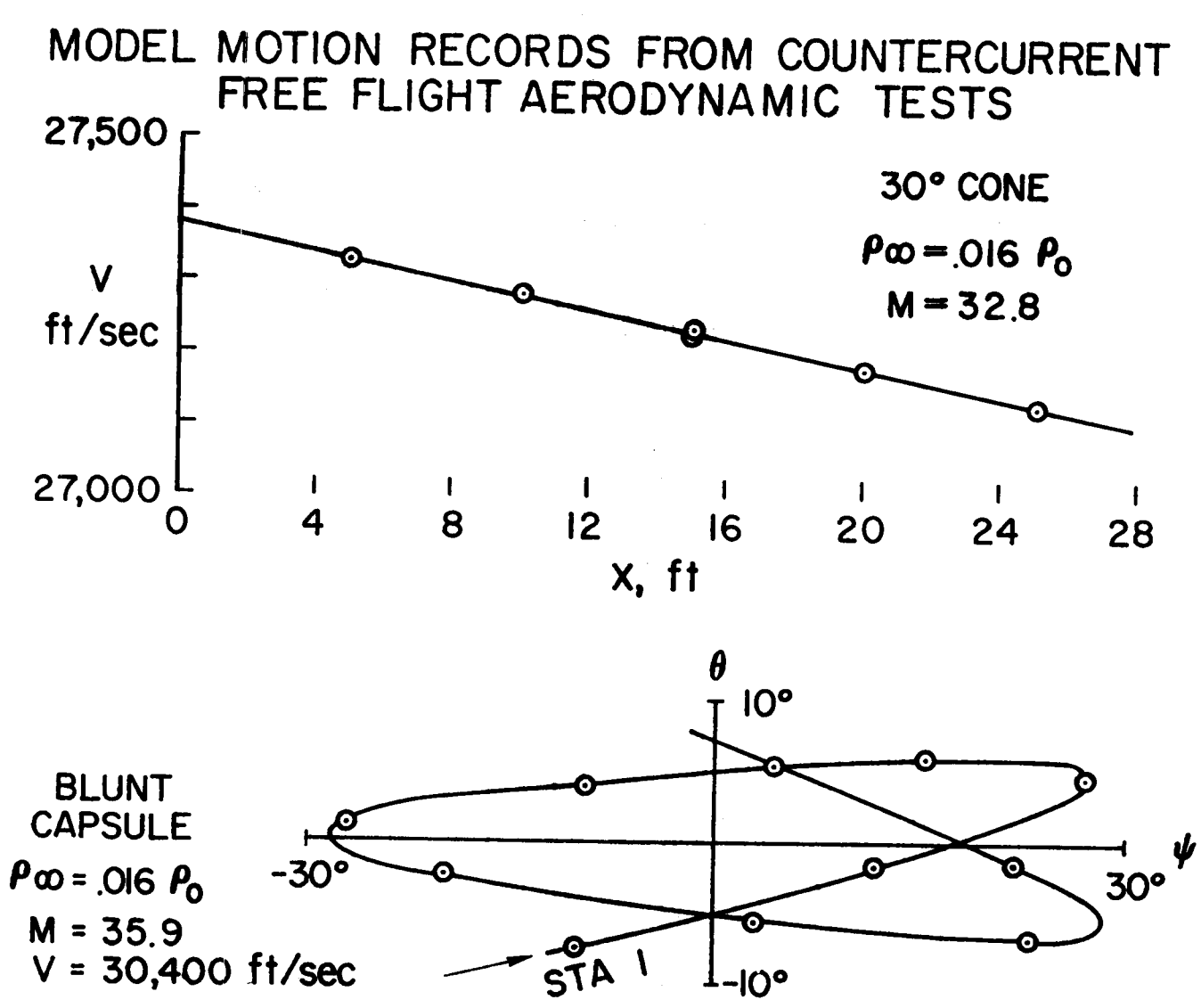

Figure 13

NATIONAL AERONAUTICS AND SPACE ADMINISTRATION
AMES RESEARCH CENTER, MOFFETT FIELD, CALIFORNIA

SHADOWGRAPHS SHOWING ONSET OF ABLATION

STATION 1
T_S = 1015° F

STATION 4
T_S = 1270° F

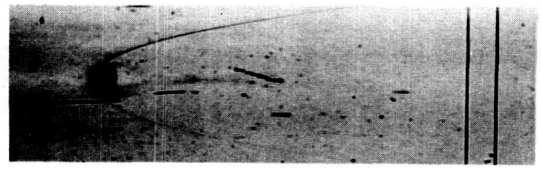

STATION 6
T_S = 1380° F

A-30645

Figure 14

NATIONAL AERONAUTICS AND SPACE ADMINISTRATION
AMES RESEARCH CENTER, MOFFETT FIELD, CALIFORNIA

CONVECTIVE HEAT TRANSFER EXPERIMENT

○ WARREN ⌂ HOSHIZAKI △ { ROSE
□ OFFENHARTZ ◆ COMPTON & COOPER { STANKEVICS & ROSE

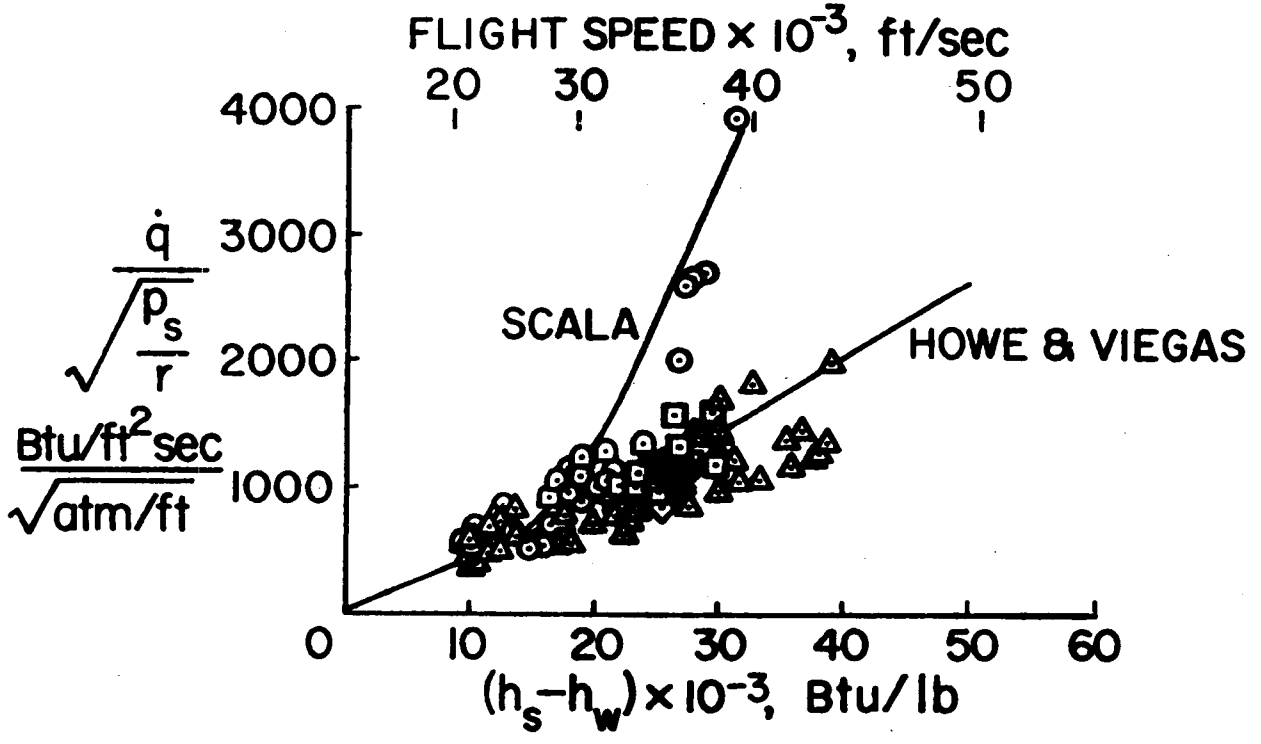

Figure 15

NATIONAL AERONAUTICS AND SPACE ADMINISTRATION
AMES RESEARCH CENTER, MOFFETT FIELD, CALIFORNIA